33rd Annual International Conference of the IEEE EMBS
Boston, Massachusetts USA, August 30 - September 3, 2011

Analysis of RF transmit performance for a 7T dual row multi-channel MRI loop array

Mikhail Kozlov, Robert Turner

Abstract— **We present a numerical investigation of the RF fields generated inside a human head by single and dual-row loop arrays. For a uniform circular polarization (CP) mode excitation, a dual-row array has no advantage for human brain excitation. Significant improvement of B_1+ homogeneity with a simultaneous increase of coverage in the axial direction can be obtained by using a dual-row array together with a static RF shim: that is, excitation of both rows separately in CP mode, while providing the upper row elements with a +90° phase shift relative to axially adjacent lower row elements. For this case the excitation efficiency over the entire brain remains practically unaffected, and the improved B_1+ coverage results in a relatively smaller amount of power delivered to brain. To keep the mean B_1+ across the brain equal to its value in a uniform CP excitation mode, a larger transmit power level is required. This results in a moderate increase of peak SAR_{10g}. The location of peak SAR_{10g} moves from the brain (uniform CP mode location) to the nose skin. The performance of dual-row arrays in transmit SENSE operation will be explored in future investigations.**

I. Introduction

MRI multi-channel arrays enable several novel applications such as B1 shimming [1] and transmit SENSE [2, 3]. Until now, most proposed array designs have been based on a single axial row of array elements. A few research groups [4, 5, 6, 7] have reported experimental results for arrays with multiple rows in the Z direction. Due to the complexity of multi-row arrays, experimental optimization alone is extremely time consuming and costly. Numerical simulation may be an important tool for array optimization, and is required to predict SAR distribution.

Most commercially available MRI scanners can be equipped with up to 8 independent transmit channels. Therefore, we investigated the effect of array loop dimension and row separation on the transmit properties of an 8-channel (twice 4 loops) dual-row loop-based 7T array. We explored dual-row array performance in circular polarization (CP) mode excitation and compared it with transmit properties of 4- and 8-channel single row arrays having the same axial length. Thereafter we applied static RF shimming (phase adjustments only) in order to explore how the degrees of freedom available in a dual-row array can benefit transmit excitation.

Our preliminary simulation results confirm that the behaviour of a dual-row array differs significantly when loaded by a human model or by simple spherical or cylindrical phantoms, due to the large asymmetry in the Z direction of the human model. Because our goal was to design an array for human head mapping we did not pursue detailed investigation of a dual-row array loaded by a simple phantom.

From our investigation of other array configurations we have learned that it is hard to predict how field and SAR maps vary with geometrical or electrical parameters. Therefore we used an manual approach similar to that used experimentally for collecting the simulation data required for reliable sensitivity analysis. Because the transmit performance and SAR depend very strongly on certain parameters, the number of parameter variations required to cover the entire parameter design space became very large. Each geometrical variation requires a separate 3-D EM simulation, which is still relatively time consuming. For this reason we focused on some major parameter dependencies.

II. Method

A. Array and load setup

RF array type #1 comprised two rows of 4 elements with identical rectangular loops, of length 70, 80 or 90 mm and angular size 85 or 75 degrees, mounted on a cylindrical acrylic former with diameter 250 or 280 mm. In some designs the first row was rotated by 45 degree relative to the second row, and/or shifted in Z direction in order to overlap the rows. Arrays type #2 and #3, used as reference designs, had only one row of 4 or 8 elements with identical rectangular loops, of length 150 mm and angular size 85 or 40 degrees respectively, mounted similarly on a cylindrical acrylic former with diameter 250 or 280 mm (Fig. 1).

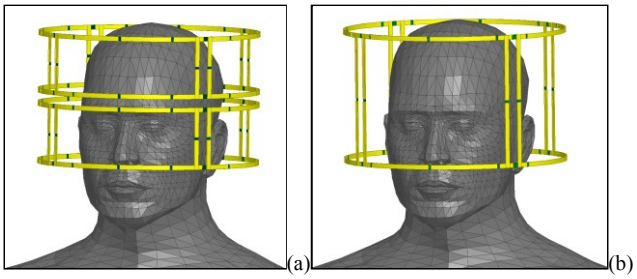

Figure 1. Model geometry setup: (a) - "type#1", (b) - "type#2"

M. Kozlov is with the Max Planck Institute for Human Cognitive and Brain Sciences, Leipzig, D-04103 Germany (corresponding author phone: +49-341-99402208; fax: +49-341-99402448; e-mail: kozlov@cbs.mpg.de).

R. Turner is with the Max Planck Institute for Human Cognitive and Brain Sciences, Leipzig, D-04103 Germany (e-mail: turner@cbs.mpg.de).

The realistic 3-D EM model of the arrays included all coil construction details for the resonance elements, simulated with precise dimensions and material electrical properties. The loads utilized were the multi-tissue Ansoft human body models, cut in the middle of the torso, with different scaling factors: a medium-size head #1 with scaling X=0.9, Y=0.9, Z=0.9, a large-size (almost fully occupying the coil volume when the diameter was 250 mm) head #2 with scaling X=0.95, Y=0.975, Z=0.9, and a small-size head #3 with scaling X=0.85, Y=0.85, Z=0.9. To investigate array transmit performance sensitivity to load position, the latter was varied in some geometrical setups.

8 capacitors (represented as green patches on the copper strip in Fig. 1) were placed in each loop to provide tune, shunt, and distributed capacitor functionality. The arrays were tuned, matched and decoupled using either capacitive or inductive decoupling approaches, or alternatively tuned by minimization of $\boldsymbol{P}_{\mathbf{array\_refl}}$ for configurations where axially adjacent array elements are decoupled by an inductive decoupling network, and elements in the same row have no dedicated decoupling network between them. The decoupling capacitors (also represented as green patches in Fig 1) connect adjacent array elements between each end of the rungs. For decoupling circumferential adjacent elements, the inductors of the decoupling networks are placed in series with a capacitor in the middle of the rungs, while for decoupling axially adjacent array elements they are placed in the middle of the loops.

The arrays were locally shielded by a cylindrical copper sheet 300 mm long, with 50 mm greater radius than the coil former. For reliable simulation of radiated power, the scanner gradient shield (a copper sheet with diameter of 683 mm and length of 1200 mm) was always included in the numerical domain.

The major limitation of the current study is the assumption of ideal common-mode-current suppression, because neither RF cable traps nor coax cable interconnection wiring have been included in the simulation domain. The results reported were obtained in somewhat idealized array design conditions: a) the values of fixed capacitors were not limited to the commercially available range, b) zero tolerance in component values was assumed, c) all tuning/matching/decoupling optimizations reached their global minima.

B. Investigation workflow

Our investigation workflow is based on RF circuit and 3-D EM co-simulation, as described in our previous report [8], where experimental validation of the workflow is also provided.

Because the decoupling network influences the value of distributed capacitors, for maximal flexibility, all distributed capacitors were substituted by lumped ports inside the 3D EM simulation domain. The RF circuit simulator was Agilent ADS, and Ansoft HFSS was chosen as the 3-D EM tool for its robustness in handling complex coil geometry and fast multi-port simulation.

To increase the reliability of simulation data, and to accelerate the simulation convergence, the 3D simulation domain was optimized by placing 3D dummy objects and refining the mesh of the human body model in regions where the gradient of electrical and magnetic fields is expected to be large. A manually variable initial mesh definition was applied. This strategy results in convergence to $\Delta S<0.002$ within not more than 3 adaptive iterations, for all 3-D EM projects of the given investigation. The number of mesh tetrahedra was as high as ~3.1 million. The entire 3-D EM simulation for frequency range of 275 to 325 MHz requires ~ 64GB computer RAM and approximately one day, using up-to-date Dell Precision T7500 Workstation.

The required values of fixed and adjustable lumped elements (capacitors, mutually coupled inductors) were obtained by a tuning/matching/decoupling procedure in the numerical domain. For the arrays with decoupling networks a set of optimization criteria is defined at the MRI resonance frequency as: a) $\boldsymbol{S}_{11}$ must be less than -40 dB, for each array element; b) coupling must be less than -20 dB, for each decoupled element pair. For optimization of $\boldsymbol{P}_{\mathbf{array\_refl}}$, criterion a) is substituted by the target criterion $\boldsymbol{P}_{\mathbf{array\_refl}}=0$.

The circuit simulator optimization procedure is guided by the error function, which calculates the difference between the actual simulation and the specifications defined by the optimization criteria. Initial guesses are made, based on numeral simulation experience, for the values of fixed and adjustable multi-channel array lumped elements, as well as the range over which adjustable elements can be varied. Then the RF circuit optimizer performs two steps: 3000 random tries, followed by "Quasi-Newton" or alternatively gradient optimization to ensure that the global minimum condition has been found. These steps take only a couple of minutes.

If the initial guess is too inaccurate, or if the range of allowed variation of adjustable element values is too large, the optimizer cannot find a converged solution. As in real life, the analysis of circuit simulation data (primary S parameter matrix and current in each array element) provides information for the direction of initial value adjustment. After this re-adjustment the RF circuit optimizer is restarted.

III. RESULTS AND DISCUSSION

A. Numerical quantities

Two volumes of interest (**VOI**) were defined: $\mathbf{VOI_1}$ - the entire human brain, and $\mathbf{VOI_2}$ - the entire cerebellum. Array transmit properties were evaluated by considering the values of $\boldsymbol{B_1}+_{\mathbf{s}}$: mean $\boldsymbol{B_1}+$ value averaged over some slices (transverse central and offset by +25 mm, central coronal) through the $\mathbf{VOI_1}$, and the inhomogeneity was defined as the ratio of $\boldsymbol{B_1}+$ rms to $\boldsymbol{B_1}+_{\mathbf{s}}$ evaluated as a percentage ("%"); $\boldsymbol{B_1}+_{\mathbf{V}}$**:** $\boldsymbol{B_1}+$ averaged over both **VOI**s, and their rms based

inhomogeneity. Parameters also evaluated were $\boldsymbol{S}$ parameter matrix, the power deposited in both **VOIs** ($\boldsymbol{P_V}$), both **VOI** excitation efficiency $\boldsymbol{B_1}+_V/\sqrt{\boldsymbol{P_V}}$ ($\boldsymbol{E_V}$), the peak SAR averaged over 10 gram ($\boldsymbol{SAR_{10g}}$), and safety excitation efficiency $\boldsymbol{B_1}+_V/\sqrt{\boldsymbol{SAR_{10g}}}$. We have not reported the ratio of $\boldsymbol{Q}_{load}/\boldsymbol{Q}_{unload}$ for the arrays investigated, , because it cannot be used for the analysis of the power deposited into the entire human model. This value, which was always more than 75% of $\boldsymbol{P_{transmit}}$, was obtained from direct integration of the power loss density within the entire human model.

Space limitations make it impossible to show all the results available from the more than 40 3-D EM simulations performed, each of which has been analyzed using several different tuning/matching/decoupling and shim arrangements. We focus on the most important findings and the relevant data.

B. Element coupling

For all designs investigated, after the optimization procedure the $\boldsymbol{S}_{11}$ (for all array elements) is below -40 dB. When inductive decoupling was used, coupling between all adjacent loops was less than -19 dB for array types #1 and #2, but was -15.5 dB for array type #3. For a type #2 array the coupling between the second neighbours was also very small (less than -20 dB). However, for type #1 without row rotation and #3 arrays with 280 mm diameter the circumferential second-neighbour coupling approached -14 dB and -10 dB respectively. Decreasing the diameter array to 250 mm resulted in reduction of the coupling just mentioned by ~1.5 dB.

Row rotation followed by inductive decoupling of both axial and circumferential adjacent elements maintains coupling between most elements at below -20dB. Only for an upper row of 280 mm in diameter, the circumferential second-neighbour coupling can approach -15 dB.

In CP excitation mode the worst case coupling has small influence on the $\boldsymbol{P}_{array\_refl}$ being less than 10% of $\boldsymbol{P_{transmit}}$.

C. Circular polarization mode excitation

At the first stage of investigation all arrays were excited using CP mode, applying 1W (2W for type #2) power to each port ($\boldsymbol{P_{transmit}}$=8W), with a sequential 90° (45° for type #3) phase increment. Phases are the same in axially adjacent array elements. This condition is labelled as shim "0" in figures and Tables from I to VI.

We use the following abbreviations for convenience: "Q1 x Q2 x Q3 x Q4 x Q5 x Q6" denotes an array configuration where: Q1 is number of rows, Q2 is the number of array elements in one row, Q3 is the angular size of the elements in degrees, Q4 is the element length in mm, Q5 indicate the separation in mm in the axial direction of the first and the second rows, and Q6 indicate rotation of the second row relative to the first one. If Q5 is negative, rows are overlapped. For single row array Q5 and Q6 are omitted. When no rotation is applied, Q6 is also omitted.

TABLE I. DIAMETER 250 MM, INDUCTIVE DECOUPLING, HEAD #1

Array configuration		**Performance measure**							
		***VOI*$_1$**				***VOI*$_2$**			
	shim	$\boldsymbol{P_V}$ W	$\boldsymbol{B_1}+_V$ μT	%	$\boldsymbol{E_V}$ μT/√W	$\boldsymbol{P_V}$ W	$\boldsymbol{B_1}+_V$ μT	%	$\boldsymbol{E_V}$ μT/√W
1x4x85x150	0	2.71	1.63	24	0.99	0.49	1.07	58	1.52
1x8x40x150	0	2.56	1.61	23	1.01	0.49	1.05	57	1.5
2x4x75x70x10	0	2.36	1.39	27	0.90	0.46	1.15	47	1.70
	+90°	1.50	1.25	16	1.02	0.52	1.36	27	1.89
	-90°	2.50	1.30	34	0.82	0.22	0.76	39	1.63
2x4x85x70x15	0	2.61	1.56	26	0.97	0.42	1.01	56	1.55
	+90°	1.62	1.30	15	1.02	0.49	1.36	32	1.95
	-90°	2.53	1.33	40	0.83	0.16	0.73	36	1.84
2x4x85x90x10	0	1.76	1.10	29	0.82	0.40	1.1	44	1.74
	+90°	1.04	1.04	20	1.02	0.47	0.97	32	1.43
	-90°	2.20	1.26	31	0.85	0.36	0.74	58	1.24
2x4x85x100x-10	0	2.28	1.30	28	0.86	0.46	1.23	42	1.81
	+90°	1.39	1.21	14	1.03	0.53	1.27	28	1.74
	-90°	2.39	1.26	33	0.82	0.24	0.74	42	1.48
2x4x85x100x-10x45	0	2.28	1.33	28	0.88	0.46	1.27	38	1.87
	+90°	1.44	1.20	16	1.01	0.51	1.36	23	1.91
	-90°	2.29	1.33	28	0.88	0.46	1.27	38	1.87

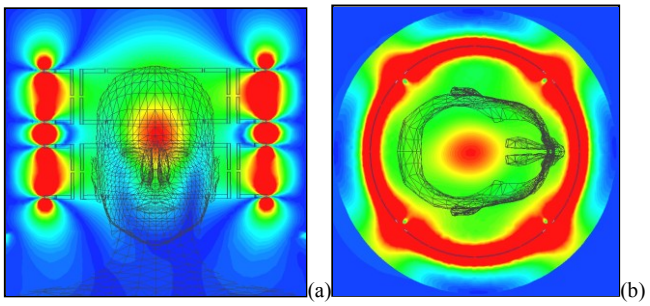
(a) (b)

Figure 2. $\boldsymbol{B_1}+$ slices for array type #1 with inductive decoupling rescaled to individual maximum: (a) - coronal, (b) - transverse

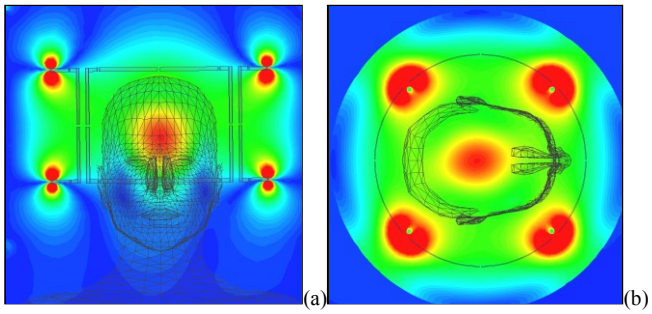
(a) (b)

Figure 3. $\boldsymbol{B_1}+$ slices for array type #2 with inductive decoupling rescaled to individual maximum: (a) - coronal, (b) - transverse

From the data in Tables I to IV, and the B1+ maps (Figs. 2 and 3) presented for the CP excitation mode (Shim 0), one can conclude that the dual-row loop array transmit properties are similar to single row loop array transmit properties, for

the same array diameter and effective array length, defined as the distance from array bottom to array top.

TABLE II. DIAMETER 280 MM INDUCTIVE DECOUPLING, HEAD #1

Array configuration		Performance measure							
		VOI_1				VOI_2			
	shim	P_V W	B_1+_V μT	%	E_V μT/√W	P_V W	B_1+_V μT	%	E_V μT/√W
1x4x85x150	0	2.60	1.60	24	0.99	0.49	1.06	57	1.52
1x4x85x170	0	2.05	1.22	29	0.85	0.44	1.23	39	1.85
1x4x85x180	0	1.94	1.17	29	0.84	0.42	1.21	29	1.85
1x8x40x150	0	2.50	1.59	23	1.01	0.49	1.05	57	1.5
2x4x85x70x15	0	2.41	1.50	25	0.97	0.39	0.99	56	1.56
	+90°	1.45	1.23	13	1.02	0.45	1.29	31	1.94
	-90°	2.22	1.24	39	0.84	0.15	0.69	37	1.76
2x4x85x80x20	0	1.78	1.16	27	0.87	0.38	1.09	43	1.77
	+90°	1.20	1.14	19	1.04	0.45	1.07	30	1.60
	-90°	1.95	1.15	33	0.82	0.27	0.68	50	1.29
2x4x85x90x20	0	1.75	1.17	26	0.89	0.36	1.02	48	1.71
	+90°	1.18	1.14	20	1.05	0.43	0.98	33	1.49
	-90°	1.92	1.18	32	0.85	0.27	0.64	61	1.22
2x4x85x100x-20	0	2.23	1.31	28	0.88	0.44	1.19	42	1.79
	+90°	1.22	1.11	14	1.01	0.46	1.21	29	1.79
	-90°	2.09	1.22	32	0.85	0.20	0.68	46	1.50
2x4x85x100x-17.5x45	0	2.25	1.37	27	0.91	0.45	1.20	41	1.79
	+90°	1.24	1.04	18	0.94	0.45	1.37	22	2.04
	-90°	2.38	1.36	33	0.88	0.27	0.64	52	1.23

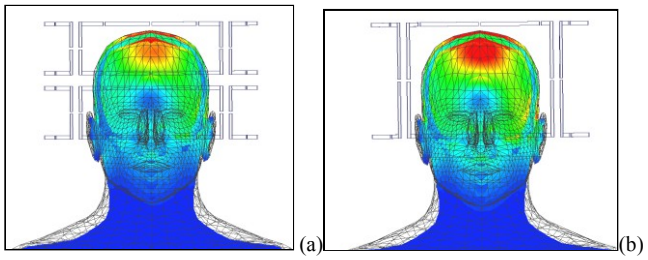

Figure 4. Power loss density for coronal slice rescaled to individual maximum: (a) - array "type#1", (b) - array "type#2"

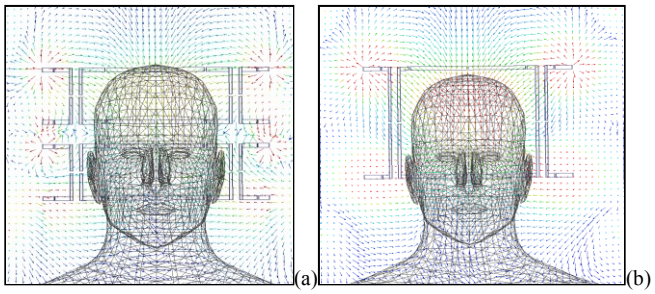

Figure 5. Real part of Poynting vector rescaled to the same maximum: (a) - array "type#1", (b) - array "type#2"

TABLE III. DIAMETER 250 MM, INDUCTIVE DECOUPLING, HEAD #1

Array configuration		Slice					
		Z 0 mm		*Z 25 mm*		*Coronal*	
	Shim	B_1+_s, μT	%	B_1+_s, μT	%	B_1+_s, μT	%
1x4x85x150	0	1.82	20	1.55	9	1.79	30
1x8x40x150	0	1.80	21	1.54	8	1.77	30
2x4x75x70x10	0	1.51	23	1.22	9	1.56	32
	+90°	1.25	9	1.39	5	1.27	14
	-90°	1.60	25	1.37	14	1.46	40
2x4x85x70x15	0	1.56	23	1.35	7	1.62	32
	+90°	1.12	9	1.45	6	1.33	15
	-90°	1.52	34	1.69	13	1.52	42
2x4x85x90x10	0	1.19	21	0.90	10	1.24	35
	+90°	1.21	10	1.06	6	1.05	20
	-90°	1.50	33	1.02	14	1.39	38
2x4x85x100x-10	0	1.39	24	1.02	11	1.45	37
	+90°	1.28	8	1.24	3	1.22	17
	-90°	1.53	25	1.21	15	1.42	39
2x4x85x100x-10x45	0	1.43	23	1.06	10	1.45	37
	+90°	1.27	10	1.22	4	1.21	18
	-90°	1.43	23	1.06	10	1.45	37

For all types of array in CP mode, most of the power is deposited in the upper part of the head, as shown in Fig. 4. As shown in Fig. 5, the electromagnetic field propagates significantly through the top of the head, and is only partly transverse to the plane of the coil elements.

TABLE IV. DIAMETER 280 MM, INDUCTIVE DECOUPLING, HEAD #1

Array configuration		Slice					
		Z 0 mm		*Z 25 mm*		*Coronal*	
	Shim	B_1+_s, μT	%	B_1+_s, μT	%	B_1+_s, μT	%
1x4x85x150	0	1.77	20	1.52	8	1.74	30
1x4x85x170	0	1.30	23	0.95	10	1.36	37
1x4x85x180	0	1.23	23	0.91	9	1.30	38
1x8x40x150	0	1.73	20	1.48	8	1.69	30
2x4x85x70x15	0	1.65	23	1.50	8	1.67	31
	+90°	1.11	8	1.33	6	1.25	15
	-90°	1.43	34	1.55	13	1.43	42
2x4x85x80x20	0	1.24	21	1.03	7	1.30	34
	+90°	1.28	9	1.25	4	1.16	20
	-90°	1.39	24	1.05	13	1.30	39
2x4x85x90x20	0	1.26	20	1.09	7	1.30	33
	+90°	1.30	10	1.26	5	1.17	22
	-90°	1.39	23	1.08	12	1.31	38
2x4x85x100x-20	0	1.42	23	1.03	11	1.45	37
	+90°	1.14	9	1.08	4	1.12	19
	-90°	1.46	25	1.22	15	1.37	39
2x4x85x100x-17.5x45	0	1.50	22	1.13	11	1.47	37
	+90°	1.02	10	1.00	5	1.02	20
	-90°	1.65	23	1.43	12	1.51	39

When each row of array type #1 is separately excited, the coronal maps of B_1+ (Fig. 6), rescaled to their individual maxima, differ significantly from each other and from the coronal B_1+ slice with simultaneous excitation of each row in CP mode.

The VOI_1 excitation efficiency differs also significantly: 0.43 μT/√W for lower row excitation and 1.02 μT/√W for upper row excitation. In other words, to achieve the same $\boldsymbol{B_1}+_V$ using the lower row, more power has to be delivered to the first **VOI**. Taking into account that the upper row is considerably closer to the first **VOI**, and that the **VOI** excitation efficiency corresponds to the MRI receiver coil signal to noise ratio (**SNR)**, our finding is in good agreement with the well-known dependence of the receiver array SNR on the separation between the receiver array and VOI. The larger the separation, the worse the SNR.

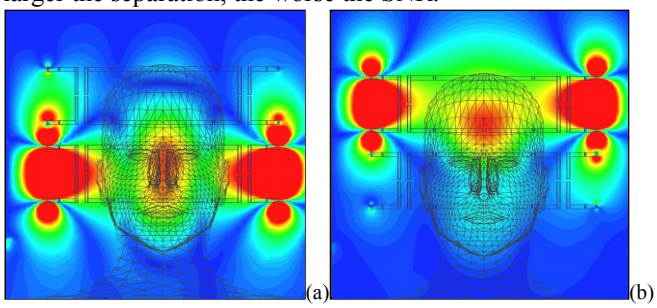

Figure 6. Coronal $\boldsymbol{B_1}+$ slices for array type #1 with inductive decoupling rescaled to individual maximum: (a) - excitation of lower row, (b) - excitation of upper row

It should be noted that the significant RF propagation within the tissue influences the maximum $\boldsymbol{B_1}+$ over the entire human model. For the lower row (field propagation in both directions) this value is 31% smaller, relative to the upper row (propagation in one direction).

After applying capacitive decoupling for circumferential adjacent elements to some designs, we found results similar to those obtained with inductive decoupling. But capacitive decoupling requires much greater effort to achieve global circuit optimization for array type #1. For this reason our entire simulation database of array type #1 has been post-processed using only inductive decoupling.

Direct minimization of $\boldsymbol{P}_{\mathbf{array\_refl}}$, with the omission of any dedicated decoupling network, has been shown [8] to provide a simple method for achieving the maximum near-field magnetic field generated per unit delivered power, for most single-row closed loop multichannel coils, independently of the design of the array radiative elements (loop, shielded microstrip, stripline). This approach fails for the multi-row array. While the method easily handles the coupling between azimuthally adjacent element (and in most cases benefits from it), there are no degrees of freedom available to compensate for axial coupling.

The reflected power minimization approach, with no dedicated decoupling network within each row, succeeds as a coil optimization method if axially adjacent array rows are explicitly decoupled by an inductive decoupling networks. The transmit properties obtained are similar to those found when all adjacent coil elements are fully decoupled.

For elements of 70 mm length there is an optimal distance, equal to 15 mm, between lower and upper row, which gives best excitation transmit performance in CP mode. If this distance is smaller or larger, then $\boldsymbol{B_1}+_V$, $\boldsymbol{P}_V$, $\boldsymbol{B_1}+_V/\sqrt{\boldsymbol{P}_V}$ for VOI_1 are slightly decreased. However, $\boldsymbol{B_1}+$ inhomogeneity over the entire brain remains almost unaffected.

Transmit performance is highly sensitive to head position within the array. An axial shift (for example of 40 mm) of the head from the optimal position for entire brain excitation can result in a significant deterioration of VOI_1 related quantities.

The results obtained allow the conclusion that in the CP excitation mode, there is no advantage for dual row array, as compared with 4 and 8 element single row arrays, either in $\boldsymbol{B_1}+$ axial coverage or homogeneity.

D. Static RF shimming

We have not yet explored a systematic approach to optimization of RF performance using sophisticated RF shimming. To obtain preliminary results regarding how simple static RF shimming can influence homogeneity on a slice-by-slice basis and axial coverage, we increased the phase of all the elements in the upper row by values in the range from -180° to + 180°. The amplitude of transmit power remained unchanged, 1W for each array element. The maximal axial $\boldsymbol{B_1}+$ maximum shift was obtained for -90° (shift to head top) and +90° (shift to head bottom), as shown in Fig. 7.

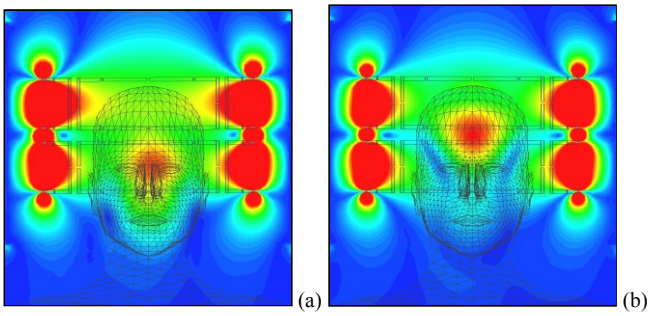

Figure 7. Coronal $\boldsymbol{B_1}+$ slices for array type #1 with inductive decoupling rescaled to individual maximum: (a) - Shim +90°, (b) - Shim -90°.

Data analysis shows that +90° static shim provides significant improvement (in most cases two fold) of $\boldsymbol{B_1}+$ homogeneity for both VOIs and all slices given (Fig. 8).

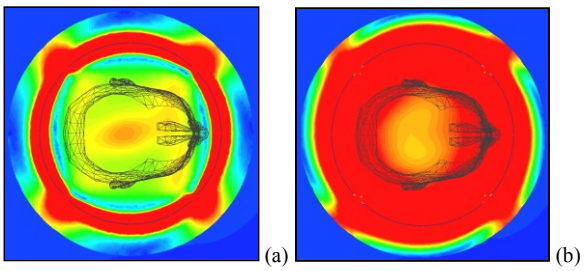

Figure 8. Shim +90°. Transverse $\boldsymbol{B_1}+$ maps, for diameter 280 mm 2x4x85x70x15 array with inductive decoupling: (a) - central plane, (b) - plane offset by +25 mm; rescaled to maximum of $\boldsymbol{B_1}+$ brain.

A similar beneficial effect is observed for a transverse

slice at Z=+60 mm, when the +90° shim is applied, as shown in Fig. 9. When this shim is applied the electromagnetic field propagates mostly in the transverse plane and only partly through the top of the head (Fig. 10a). The result is that only a small amount of the power is deposited in the brain at the top of the head, as shown in Fig. 10b.

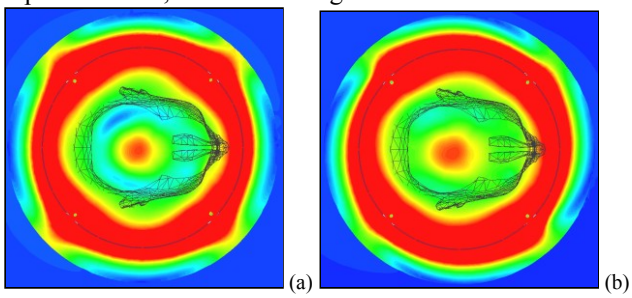

Figure 9. Transverse B_1+ plane at Z=+60mm, for diameter 280 mm 2x4x85x70x15 array with inductive decoupling rescaled to individual maximum: (a) - Shim=0°, max=1.76 μT , (b) - Shim=+90°, max=1.88 μT

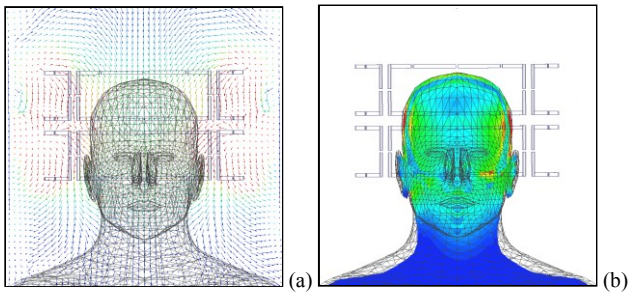

Figure 10. Coronal slices for array type #1 with excitation of upper row with +90° phase shift: (a) - real part of Poynting vector, (b) - power loss density

For some designs the -90° static shim provides a somewhat better transmit performance for particular quantities, but this static shim value does not appear to reduce the B_1+ inhomogeneity for both VOIs as much as the +90° static shim does.

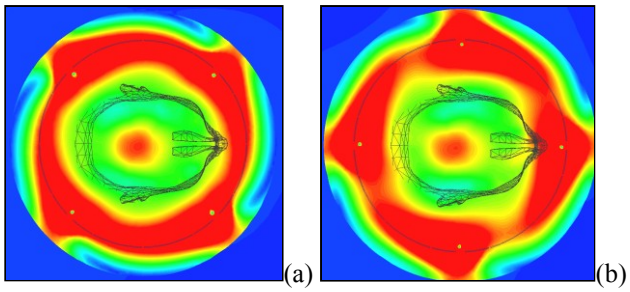

Figure 11. Transverse B_1+ plane at Z=+60mm, for diameter 280 mm arrays with inductive, Shim=+90°, rescaled to individual maximum: (a) - 2x4x85x100x-20, max=1.88 μT, (b) -2x4x85x100x-17.5x45, max=2.01 μT

A rotation of 45 degrees between the rows results in more effective excitation of VOI_2 – the cerebellum, located close to the back of the head - (Fig. 11) and VOI_1 for 280 mm diameter array (Table II) when shim +90° is applied. Thus relative array rotation provides an additional degree of freedom available for dual-row array optimization.

An arbitrary but identical phase shift can be applied for all elements of the second row for an array tuned by minimization of P_{array_refl} with axially adjacent array elements decoupled. Applying -90° and +90° shim provides results similar to the simulation data for an entirely inductively decoupled array. This tuning arrangement is included in our investigation because it provides significantly improved load independence relative to capacitive or inductive decoupling approaches, if only static RF shim between rows is applied.

E. SAR analysis

As expected, static transmit shimming significantly affects SAR_{10g} (both peak value and peak location) as shown in Fig. 12 and Tables V and VI. But from the MRI perspective, it is the level of safe excitation efficiency that defines MRI scanner performance, not the peak SAR_{10g}, which we have included for comparison with other results. Relative to CP excitation, when the +90° shim is applied, there is about 15% decrease of VOI_1 safety excitation efficiency - $B_1{+}_V/\sqrt{SAR_{10g}}$ and SAR_{10g} peak moves from head brain to area closed to the nose skin.

TABLE V. DIAMETER 250 MM, INDUCTIVE DECOUPLING, HEAD #1

Array configuration	Shim	SAR_{10g} W/kg	VOI_1 $B_1{+}_V/\sqrt{SAR_{10g}}$ μT/√(W/kg)	VOI_2 $B_1{+}_V/\sqrt{SAR_{10g}}$ μT/√(W/kg)	SAR_{10g} location X mm	Y mm	Z mm
1x4x85x150	0	4.82	0.74	0.49	2	-7	-41
1x8x40x150	0	4.61	0.75	0.49	2	-7	-41
2x4x75x70x10	0	4.79	0.63	0.52	35	88	56
	+90	4.61	0.58	0.63	-22	-59	55
	-90	5.75	0.54	0.32	2	-8	-41
2x4x85x70x15	0	4.88	0.71	0.46	-2	-9	-41
	+90	4.65	0.60	0.63	19	93	69
	-90	7.24	0.49	0.27	0	-6	-42
2x4x85x90x10	0	3.63	0.58	0.58	31	88	58
	+90	4.40	0.50	0.46	-16	90	48
	-90	4.14	0.62	0.36	28	91	48
2x4x85x100x-10	0	4.26	0.63	0.59	35	88	56
	+90	4.47	0.57	0.60	-20	-59	53
	-90	5.17	0.56	0.33	2	-7	-41
2x4x85x100x-10x45	0	3.46	0.72	0.68	5	-8	-26
	+90	5.76	0.50	0.57	6	101	55
	-90	5.26	0.56	0.33	2	-7	-41

It should be noted that for an array 280 mm in diameter with specification 2x4x85x70x15 , the VOI_2 safety excitation efficiency increases by 40%. Taking into account that VOI_2 excitation efficiency - $B_1{+}_V/\sqrt{P_V}$ also increases for this array when the +90° shim is applied, this design may be the most suitable transmit array when it is desired to investigate both

brain and cerebellum simultaneously with MRI.

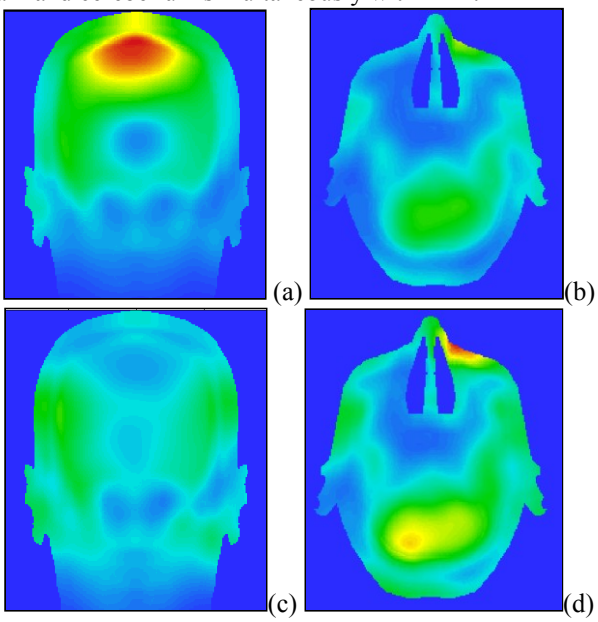

Figure 12. SAR_{10g} for 2x4x85x70x15 with inductive decoupling at coronal ("a" and "c") and transverse planes; ("a" and "b") - shim=0, ("c" and "d") - shim=+90°

TABLE VI. DIAMETER 280 MM, INDUCTIVE DECOUPLING, HEAD #1

Array configuration			VOI_1	VOI_2	SAR_{10g} location		
	Shim	SAR_{10g} *W/kg*	$B_1+_V/\sqrt{SAR_{10g}}$ $\mu T/\sqrt{(W/kg)}$	$B_1+_V/\sqrt{SAR_{10g}}$ $\mu T/\sqrt{(W/kg)}$	*X mm*	*Y mm*	*Z mm*
1x4x85x150	0	4.57	0.75	0.50	2	-8	-41
1x4x85x170	0	4.05	0.61	0.61	35	88	56
1x4x85x180	0	4.02	0.58	0.60	35	88	56
1x8x40x150	0	4.21	0.76	0.50	0	-8	-41
2x4x85x70x15	0	4.42	0.72	0.47	-2	-8	-41
	+90	3.86	0.62	0.66	19	93	69
	-90	6.27	0.50	0.27	0	-6	-42
2x4x85x80x20	0	3.30	0.64	0.60	35	88	56
	+90	3.50	0.61	0.57	-19	-59	53
	-90	3.87	0.59	0.34	2	-7	-41
2x4x85x90x20	0	3.25	0.65	0.57	35	88	56
	+90	3.31	0.63	0.54	-15	91	45
	-90	3.76	0.61	0.33	-2	-6	-41
2x4x85x100x-20	0	3.85	0.67	0.61	31	88	58
	+90	3.82	0.60	0.62	-2	-59	54
	-90	4.72	0.56	0.31	2	-7	-41
2x4x85x100x-17.5x45	0	5.11	0.61	0.53	4	104	55
	+90	3.46	0.56	0.74	5	-8	-26
	-90	5.68	0.57	0.27	2	-7	-41

IV. CONCLUSION

The presented simulation setup allows investigation of a multi-row array with inductive and capacitive decoupling network, or alternatively with no dedicated decoupling network between circumferential adjacent elements, on the basis of a single 3-D simulation followed by an RF circuit/3D EM co-simulation for the given decoupling approach and static shim condition. The HFSS frequency-domain solver was found to be a vital tool for multi-channel RF coil investigation, because simulation of a 80 port project using time-domain tools is significantly longer for similar computer hardware and license configurations.

The simulation data base obtained does not cover the entire sensitivity analysis simulation space, but it allows discovery of some important dependencies regarding dual-row array transmit performance.

Eight dual row elements are insufficient for parallel receiving with a high acceleration factor. Thus the dual-row design recommended here is more suitable as the transmit part of a transmit-only receive-only MRI array.

Extension of this simulation data base, guided by experimental validation of the findings obtained, the results derived from sophisticated static RF shimming optimization of both transmit amplitudes and phases, as well as calculation of transmit SENSE pulses and worst case SAR analysis, should be performed before final decisions regarding coil configuration are made.

REFERENCES

[1] TS. Ibrahim, YK. Hue, L. Tang, " Understanding and manipulating the RF fields at high field MRI," NMR Biomed., 22(9), pp.927-936, Nov 2009.

[2] U. Katscher, P. Börnert, " Parallel RF transmission in MRI," NMR Biomed, 19(3), pp. 393-400, May 2006.

[3] Z. Zhang, CY. Yip, W. Grissom, DC. Noll, FE. Boada, VA. Stenger, "Reduction of transmitter B1 inhomogeneity with transmit SENSE slice-select pulses," Magn Reson Med., 57(5), pp. 842-847, May 2007.

[4] G. Adriany, J. Ritter, T. Vaughan, K. Ugurbil, P.-F. Van de Moortele, "Experimental Verification of Enhanced B1 Shim Performance with a Z-Encoding RF Coil Array at 7 Tesla," Proceedings of the 18th Annual Meeting, 2010, p. 3831, May 2010.

[5] KM Gilbert, AT Curtis, JS Gati, LM Klassen, RS Menon, "A radiofrequency coil to facilitate B(1) (+) shimming and parallel imaging acceleration in three dimensions at 7 T," NMR Biomed, Dec 8 2010. [Epub ahead of print]

[6] Wiggins GC, Mareyam A, Setsompop K, Alagappan V, Potthast A, Wald LL, " A close-fitting 7 Tesla 8 channel transmit/receive helmet array with dodecahedral symmetry and B1 variation along," Proceedings of the 16th Annual Meeting of ISMRM, Toronto, ON, Canada, p. 148, May 2008.

[7] Avdievich N., Pan J., and Hetherington H., "Improved longitudinal coverage for human brain at 7T: A 16 Element Transceiver Array," Proceedings of the 19th Annual Meeting of ISMRM, Montreal, Canada, p. 328, May 2011.

[8] M. Kozlov, R. Turner, "Fast MRI coil analysis based on 3-D electromagnetic and RF circuit co-simulation," J. Magn. Reson., vol. 200, pp. 147-152, Sep. 2009.